Available online at www.sciencedirect.com
SCIENCE DIRECT®
Tetrahedron
Tetrahedron 60 (2004) 3097–3107

Synthesis of a complementary dimer from mono(imidazolyl)-substituted cobalt(II) porphyrin as a new artificial T-form hemoglobin

Yusuke Inaba[a] and Yoshiaki Kobuke[a,b,*]

[a]*CREST, Japan Science and Technology Agency (JST), Japan*
[b]*Graduate School of Materials Science, Nara Institute of Science and Technology, 8916-5 Takayama, Ikoma 630-0192, Japan*

Received 8 December 2003; revised 22 January 2004; accepted 23 January 2004

Abstract—Mono(imidazolyl)-substituted Co(II) porphyrin dimer with a 'picket fence' structure was synthesized as a new artificial hemoglobin model containing two binding sites. The dimer was confirmed by UV–vis, resonance Raman and ESR spectral measurements to bind two dioxygen molecules reversibly. The dioxygen binding affinity of the dimer was lower than that of the corresponding monomer. The decrease in this affinity is discussed in terms of steric hindrance and orientational effect of the axial ligand.

1. Introduction

We have reported previously that zincporphyrin having an imidazolyl group at the *meso* position could form a complementary dimer, where each imidazolyl group was coordinated to the Zn(II) ion of the other porphyrin in a slipped cofacial arrangement.[1] This coordination organization was sufficiently strong that the stability constant was estimated to be $10^{10}\,M^{-1}$ in $CHCl_3$, and the dimer was the structural and functional mimic of the special pair in the reaction center of bacterial photosynthesis.[1,2] The aim of this research is to use the complementary dimer of mono(imidazolyl)-substituted Co(II) porphyrin as a dioxygen carrier with two binding sites in a molecule that mimics the multi-binding sites of hemoglobin. The creation of a 'picket fence' Co(II) porphyrin, *meso*-tetrakis(α,α,α,α-*o*-pivalamidophenyl)porphyrinatocobalt(II), $Co^{II}Piv_4P$, has opened an ingenious approach to reversible dioxygen binding even at room temperature by sterically blocking the formation of the μ-oxo dimer and stabilizing the dioxygen adduct through hydrogen bonding in the picket fence cavity.[3–8]

In this report, complementary dimer formation was combined with the picket fence strategy to prepare a *meso*-[mono(2-imidazolyl)-tris(α,α,α-*o*-pivalamidophenyl)]porphyrinatocobalt(II) dimer, **5D**, $(Co^{II}Piv_3ImP)_2$ (Scheme 1). Some dioxygen carrier models, which provided two binding sites from a porphyrin dimer, have been reported in the literature. Examples include gable porphyrin,[9] dimeric picket fence porphyrin,[10] Traylor's porphyrin system,[11] and 'looping-over' porphyrin systems.[12] The new model described in this report is different from these dimeric models with regard to two structural points. Gable porphyrin and dimeric picket fence porphyrin systems require the addition of excess bidentate bases as axial ligands. On the other hand, dimer **5D** does not need the addition of external axial ligands in a similar way to looping-over porphyrin systems. Axial ligands are provided from another imidazolyl-substituted porphyrin component of the complementary dimer, and dioxygen binding sites can be constructed solely from the porphyrin component. The addition of excess external axial ligand frequently causes oxidation of Co(II) porphyrin. This factor also favors the model reported in this report. Secondly, the distance between the two porphyrin components of dimer **5D** is shorter than that of looping-over porphyrin systems, and is the shortest among the various dimer models reported. Based on these considerations, dimer **5D** was expected to be a new dioxygen carrier model with two binding sites in immediate proximity to the molecule.

In this paper, the reversible binding of two dioxygen molecules to two binding sites of dimer **5D** at low temperature is reported. Although the oxygen affinity of dimer **5D** was significantly decreased compared with the monomer, this novel dimer **5D** could be regarded as a T-form model of hemoglobin.

Keywords: Artificial hemoglobin; Porphyrin dimer; Picket fence cobalt porphyrin; Dioxygen binding; Oxygen affinity.
* Corresponding author. Address: Graduate School of Materials Science, Nara Institute of Science and Technology, 8916-5 Takayama, Ikoma 630-0192, Japan. Tel.: +81-743726110; fax: +81-743726119;
e-mail address: kobuke@ms.aist-nara.ac.jp

0040–4020/$ - see front matter © 2004 Elsevier Ltd. All rights reserved.
doi:10.1016/j.tet.2004.01.066

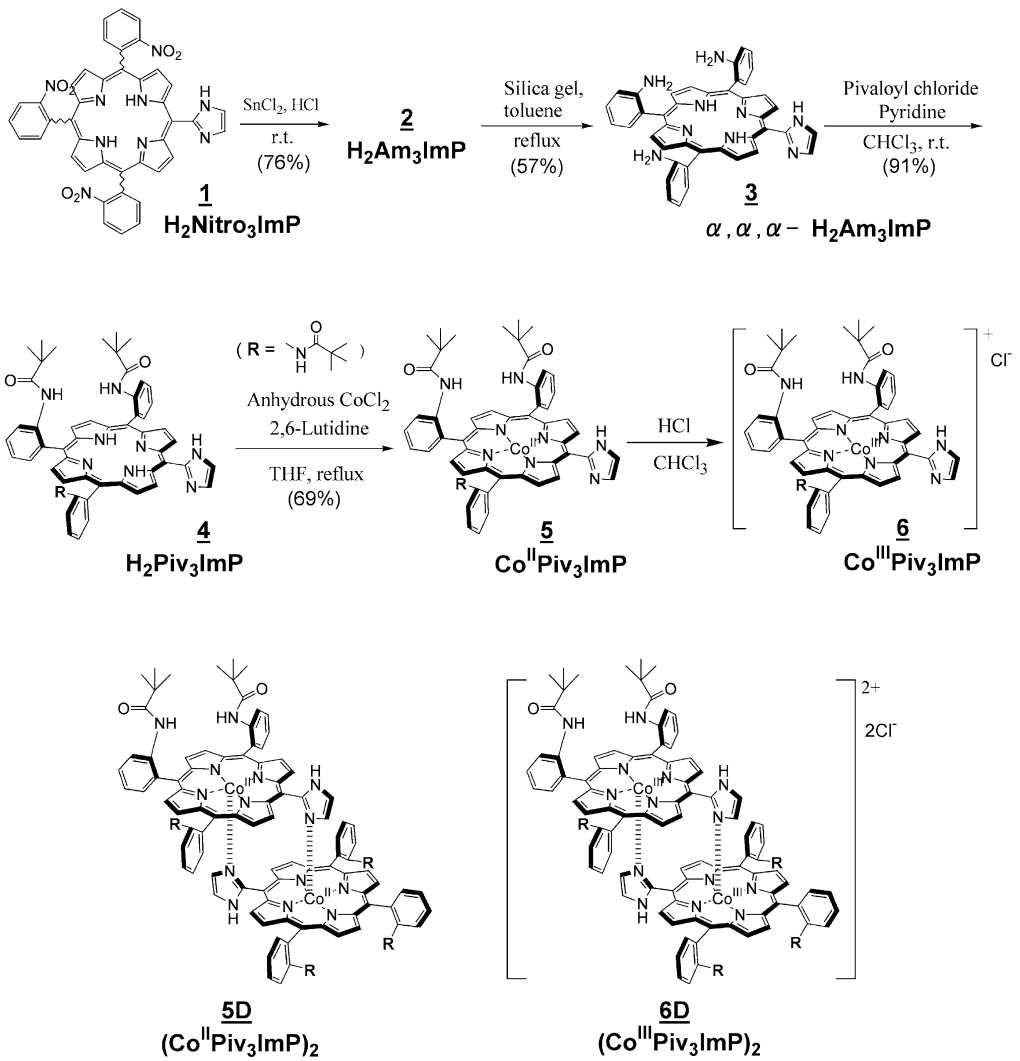

Scheme 1. Synthetic route to mono(imidazolyl)-substituted Co(II) porphyrin with a picket fence structure.

2. Results and discussion

2.1. Synthesis

Synthetic routes to mono(imidazolyl)-substituted picket fence Co(II) porphyrin **5**, $Co^{II}Piv_3ImP$, were referenced to the synthesis of picket fence porphyrins,[5,6] as is shown in Scheme 1. The starting porphyrin, 5-(2-imidazolyl)-10,15,20-tris(*o*-nitrophenyl)porphyrin, **1**, H_2Nitro_3ImP was obtained by the annelation reaction from pyrrole, 2-nitorobenzaldehyde, and imidazole-2-carboxaldehyde[13] (in a ratio of 3:2:1), in 8% yield. H_2Nitro_3ImP was reduced to aminophenylporphyrin, **2**, H_2Am_3ImP, by $SnCl_2{\cdot}2H_2O$ in conc. HCl at room temperature. The reduction of *meso*-tetrakis(*o*-nitrophenyl)porphyrin, H_2Nitro_4P, to *meso*-tetrakis(*o*-aminophenyl)porphyrin, H_2Am_4P, was effected by heating at 65–70 °C, following literature methods.[5] However, the same approach could not be applied to the reduction of H_2Nitro_3ImP, **1**. MALDI-TOF mass spectroscopy of the product obtained at 65–70 °C suggested over-reduction, and the UV–vis spectrum did not show the expected pattern of Soret and Q bands. Accordingly, the adduct was kept at room temperature for 30 min and the resulting product gave the mass $(M+H)^+$ in the MALDI-TOF mass spectrum, and the Soret and Q bands of the UV–vis spectrum were those expected of H_2Am_4P. H_2Am_3ImP, **2**, was obtained in 56% yield as a mixture of three atropisomers assigned tentatively as α,α,β-, α,β,α- and α,α,α-isomers. The mixture of atropisomers was isomerized to α,α,α-H_2Am_3ImP, **3**, by refluxing with silica gel in toluene under Ar.[14] The conversion of atropisomers was monitored by thin-layer chromatography on silica gel (TLC) (eluent $CHCl_3$/MeOH, 9:1) and reversed-phase high performance liquid chromatography (HPLC) (column TSK-gel Octadecyl-4PW (TOSHO); eluent MeOH/H_2O, 9:1, 0.8 mL/min). Before the reaction, one spot appeared at R_f=0.55 in TLC, and three peaks were detected in HPLC at 3.6, 3.9 and 6.2 min (in a ratio of about 5:5:1). After the reaction, the spot at R_f=0.55 disappeared almost completely and a new spot at R_f=0.50 appeared on the TLC, and in the HPLC, the two peaks at 3.6 and 3.9 min decreased and the peak at 6.2 min increased notably (in a ratio of about 1:4:20). The new compound, which appeared as a spot at R_f=0.50 in TLC with a retention time of 6.2 min in HPLC, was assigned as the α,α,α-isomer. The TLC spot at R_f=0.50 was the most polar product among three atropisomers, as expected from molecular dipole considerations by analogy with α,α,αα-H_2Am_4P.[5] The reason for the polarity reversal

in the reversed-phase HPLC against the TLC is not known. α,α,α-H_2Am_3ImP, **3**, was purified by silica gel column chromatography to give the product in 57% yield, and then this was reacted with pivaloyl chloride according to established methods.[5] As a result, monoimidazolyl picket fence porphyrin, H_2Piv_3ImP, **4**, was obtained in 88% yield, and treated with anhydrous $CoCl_2$ and 2,6-lutidine[6] to afford $Co^{II}Piv_3ImP$, **5**. $Co^{II}Piv_3ImP$ was oxidized to $Co^{III}Piv_3ImP$, **6**, by treatment with dilute HCl for the purpose of examining in detail the structure by NMR spectroscopy.

2.2. Structural elucidation of $Co^{III}Piv_3ImP$

We examined first the structure of *meso*-[mono(2-imidazolyl)-tris(α,α,α-*o*-pivalamidophenyl)]porphyrinatocobalt(III), $Co^{III}Piv_3ImP$, **6**. Liquid chromatography/high-resolution electrospray ionization mass spectra (LC/HRESI(+)MS) of the $CHCl_3$ solution of $Co^{III}Piv_3ImP$, **6**, gave two peaks corresponding to a monomer and a dimer with a relative intensity of 1:0.16, respectively. This mass spectroscopic data suggested that dimeric porphyrin **6D** was formed by complementary coordination of imidazolyl to Co(III) in $CHCl_3$. The UV–vis absorption spectrum of $Co^{III}Piv_3ImP$ in $CHCl_3$ showed a broad Soret band at 434 nm (half peak width of 45 nm) and a Q band at 554 nm, as shown in Figure 1. The broad Soret band may have arisen from the exciton interaction of the slipped cofacial dimeric structure of **6D**, $(Co^{III}Piv_3ImP)_2$, in nonpolar media, by analogy, had split bands for the imidazolyl-substituted Zn porphyrin dimer.[1]

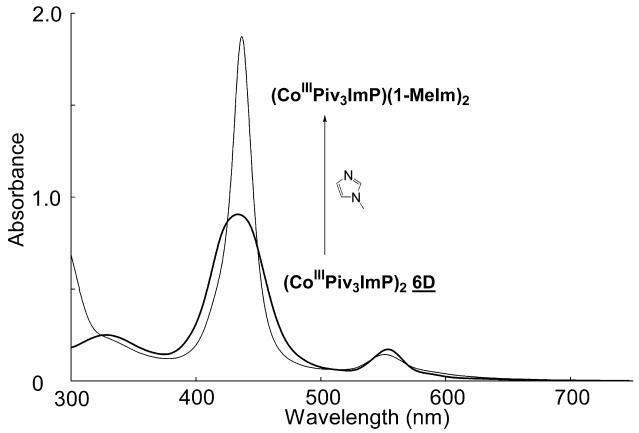

Figure 1. UV–vis spectra of $(Co^{III}Piv_3ImP)_2$ **5D** (bold line) and $(Co^{III}Piv_3ImP)(1\text{-MeIm})_2$ (narrow line) in $CHCl_3$.

The ^1H NMR spectrum (600 MHz, $CDCl_3$) of $Co^{III}Piv_3ImP$ was assigned carefully with help of H–H COSY spectra, with reference to the spectra of free-base porphyrin, H_2Piv_3ImP (Figs. 2 and 3). The protons of the phenyl and pivaloyl groups were readily assigned because the chemical shifts of these peaks resembled those of H_2Piv_3ImP and H_2Piv_4P. Distinctive differences between $Co^{III}Piv_3ImP$ and H_2Piv_3ImP were observed at the chemical shifts of the β-pyrrole and imidazole protons. All β-pyrrole protons of H_2Piv_3ImP were observed at 8.80 (4H, C12-, C18–H and C13-, C17–H), 8.83 (2H, C2-, C8–H) and 9.03 ppm (2H, C3-, C7–H; integral values are based on the monomer structure). In $Co^{III}Piv_3ImP$, on the other hand, the doublet peaks at 5.36–5.41, 8.43, 9.11 and 9.22 ppm were assigned as β-pyrrole protons. If $Co^{III}Piv_3ImP$ forms a slipped cofacial dimer, C3-, C7–H and C2-, C8–H should be considerably influenced by ring current effects from another porphyrin and appear at higher magnetic field.[1,2] The peaks at 5.36–5.41 and 8.43 ppm were correlated to each other in COSY, and the peaks at 5.36–5.41 and 8.43 ppm were assigned to C3-, C7–H's and C2-, C8–H's, respectively. Especially, C3-, C7–H's at 5.36–5.41 ppm were located above another porphyrin ring, receiving the ring current effect more efficiently than C2- and C8–H at 8.43 ppm. However, the peak integration at 5.36–5.41 ppm corresponded not to 2H but to 3H, and these peaks were correlated with two peaks at 0.66 (d, 1H) and 8.79 ppm (s, 1H) in COSY. It was thought that the peaks at 5.36–5.41 ppm might be overlapped with C22–H (imidazole). A doublet peak at 0.66 ppm, which correlated with a peak at 5.36–5.41 ppm in COSY, was assigned as C23–H, which was in the closest contact with another porphyrin. A broad singlet peak at 8.79 ppm was assigned as N5–H, because this peak correlated to the peak at 5.36–5.41 ppm in COSY and did not correlate to any other peaks of the ^{13}C NMR in HMQC. These shifts of β-pyrrole and imidazole protons to higher magnetic fields indicated the formation of the slipped cofacial dimer $(Co^{III}Piv_3ImP)_2$, **6D**, since the shielding by the second porphyrin ring current (a 'dimerization-induced shift'[1,15]) should be maximized. Imidazole protons (C22–H and C23–H) of H_2Piv_3ImP were observed at ~7.8 ppm as a broad single peak, because the imidazolyl group could rotate freely. In the case of $Co^{III}Piv_3ImP$, the imidazole protons were observed as two peaks. This differences also proved the formation of the dimeric structure, because the rotation was inhibited in $(Co^{III}Piv_3ImP)_2$, **6D**, by coordination of N6 to the cobalt of another porphyrin. These assignments are summarized in Figure 3.

Addition of excess 1-methylimidazole (1-MeIm) to dimer **6D** was expected to generate the monomeric species by competitive coordination. However, when $(Co^{III}Piv_3ImP)_2$ was dissolved in $CHCl_3$/1-MeIm=3:1, the UV–vis spectrum changed only very slowly. Even after a day, the spectrum continued to change. Therefore, this solution, Co^{III} complex in $CHCl_3$/1-MeIm, was concentrated once slowly, and redissolved in $CHCl_3$/1-MeIm=3:1. This time, the spectral change came to completion. The broad Soret band of $(Co^{III}Piv_3ImP)_2$ at 434 nm (half peak width of 45 nm) became sharp and shifted to 437 nm (half peak width of 21 nm), accompanied with shifts of the Q-bands to 551 from 554 nm (Fig. 1). The final sharp Soret band should have corresponded to that of the monomer by dissociation of the dimeric structure. The fact of the monomeric structure was confirmed by analyzing the ^1H NMR spectrum. The characteristic overlap of β-pyrrole (C3, C7–H) and imidazole (C22–H) protons at 5.36–5.41 ppm observed for $(Co^{III}Piv_3ImP)_2$, **6D**, disappeared completely. Therefore, $(Co^{III}Piv_3ImP)_2$, **6D**, was dissociated to the monomer by the addition of excess 1-MeIm to form the bis(1-MeIm) complex, $(Co^{III}Piv_3ImP)(1\text{-MeIm})_2$.

In order to obtain further evidence of the formation of the dimeric structure, the elution behavior in gel-permeation

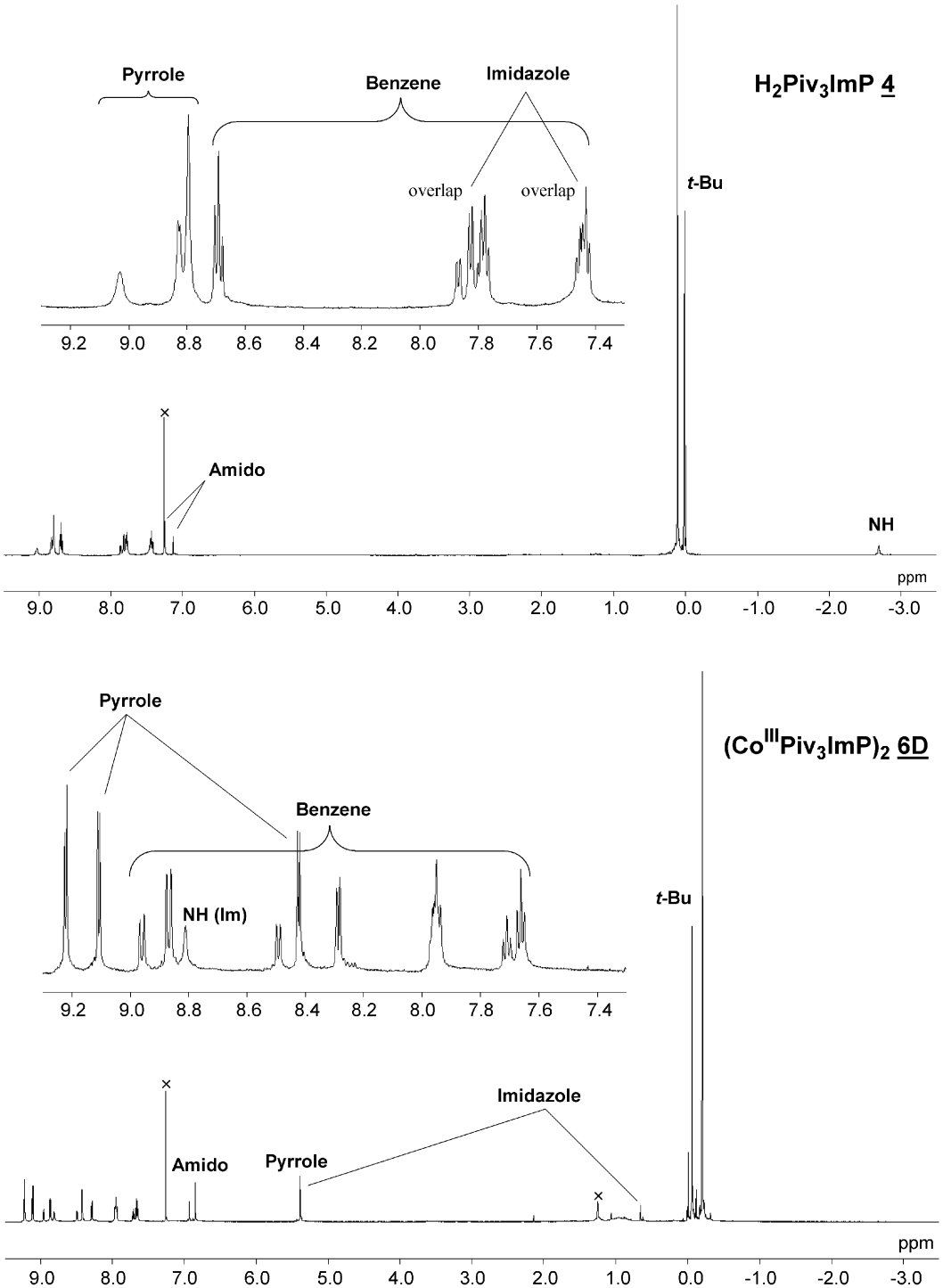

Figure 2. ^{1}H NMR spectra (600 MHz, $CDCl_3$) of H_2Piv_3ImP **4** and $(Co^{III}Piv_3ImP)_2$ **6D**.

chromatography (GPC) using a column with an exclusion limit of 2×10^4 Da was studied. This technique has been successfully applied to differentiating imidazolyl-substituted zincporphyrin oligomers.[2] For $(Co^{III}Piv_3ImP)_2$, **6D**, a sharp elution peak, with the same UV–vis spectrum shown in Figure 1, appeared at 10.7 min, which was a shorter retention time than that of $(Co^{III}Piv_3ImP)(1\text{-}MeIm)_2$, at 13.1 min (Fig. 4). This result supported the notion that $Co^{III}Piv_3ImP$, **6**, existed predominantly as a dimer, $(Co^{III}Piv_3ImP)_2$, **6D**.

2.3. Structural elucidation of $Co^{II}Piv_3ImP$

LC/HRESI(+)MS of the $CHCl_3$ solution of $Co^{II}Piv_3ImP$, **5**, gave two peaks corresponding to a monomer and a dimer, the latter with an intensity of 13% relative to that of the monomer. This mass spectral data also suggested that the dimeric porphyrin existed in $CHCl_3$, analogous to $Co^{III}Piv_3ImP$. The ^{1}H NMR spectrum of $Co^{II}Piv_3ImP$ in CD_2Cl_2 showed four broad peaks ascribable to the β-pyrrole protons at 7.5, 9.2, 12.2, and 13.8 ppm. In the case of

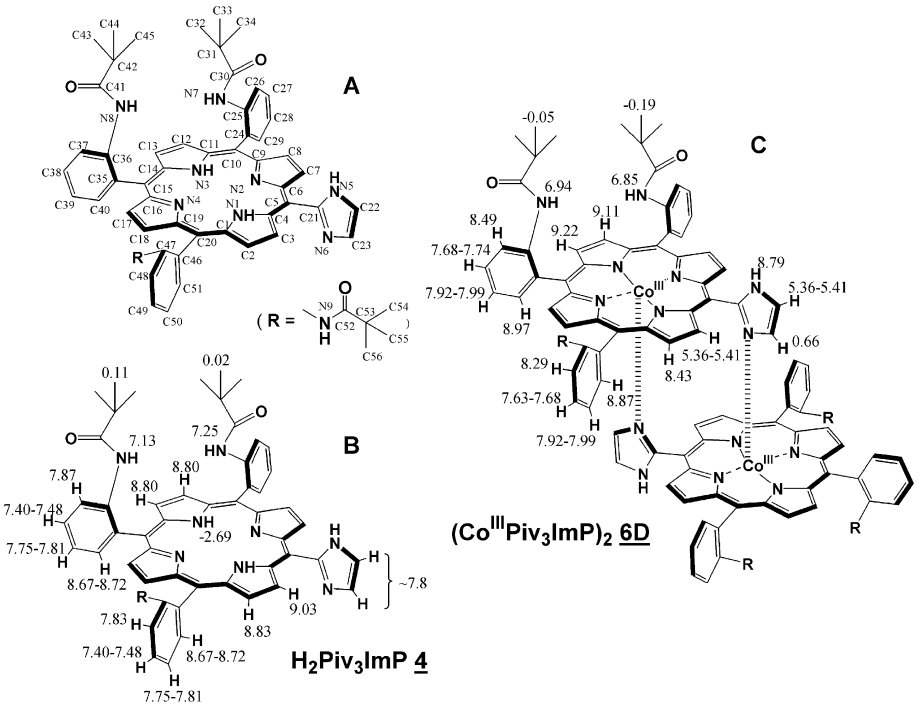

Figure 3. Chemical shifts data of H_2Piv_3ImP **4** and $(Co^{III}Piv_3ImP)_2$ **6D** in ^1H NMR (600 MHz, $CDCl_3$). Numerical values in **B** and **C** show the assignment of chemical shifts (ppm).

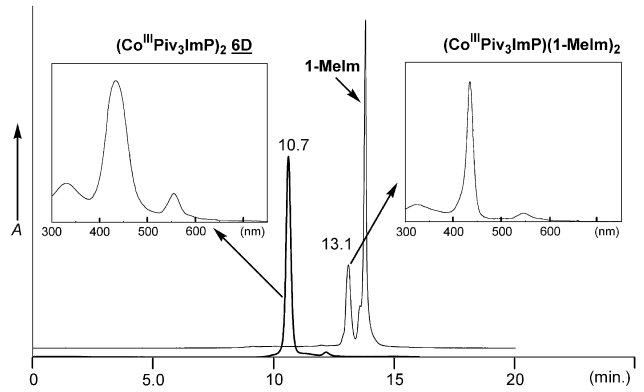

Figure 4. GPC analysis of $(Co^{III}Piv_3ImP)_2$ **6D** (bold line) and $(Co^{III}Piv_3ImP)(1\text{-MeIm})_2$ (narrow line) using a column (JAIGEL-2.5 HA) with an exclusion limit of 2×10^4 Da (eluent; $CHCl_3$, flow rate; 1.2 mL/min, detection; absorption at 420 nm). The UV–vis spectra of peaks at 10.7 and 13.1 min are shown as insets.

Co^{II}TPP-(pyridine-d_5), the β-pyrrole protons' signal appeared at 12.5 ppm as a single broad peak.[16] Therefore, the four broad peaks of $Co^{II}Piv_3ImP$ may be influenced anisotropically by a 'dimerization-induced shift'. However, we could not assign definitely these four peaks and imidazolyl protons because no correlation peaks were observed in H–H COSY and HMQC because of peak broadening.

Formation of the dimeric structure of $(Co^{II}Piv_3ImP)_2$, **5D**, was also suggested from 1-MeIm titration in CH_2Cl_2 (Fig. 5). The UV–vis absorption spectrum of $Co^{II}Piv_3ImP$ in CH_2Cl_2 under N_2, Figure 5A-a, showed a broad Soret band at 409 nm (half peak width of 42 nm) with a shoulder at 389 nm and a Q band at 534 nm. With the addition of 1-MeIm, this broad Soret band became sharp and shifted to 412 nm (half peak width of 25 nm), accompanied by shifts of the Q-bands from 534 to 531 nm. The final spectrum resembled that of $Co^{II}Piv_4P$ with axial coordination from 1-MeIm with respect to the half band width and the peak maxima. The resultant species was assigned as monomer **7** with an axial ligation by 1-MeIm, $(Co^{II}Piv_3ImP)(1\text{-MeIm})$. The initial mono(imidazolyl)-substituted Co(II) complex corresponded to the slipped cofacial dimer **5D** in CH_2Cl_2. This corresponds to Eq. 1 and the other related coordination equilibria, which are expressed as follows:

$$(CoPiv_3ImP)_2 + 2Im \overset{K_a}{\rightleftharpoons} 2(CoPiv_3ImP)Im \quad (1)$$

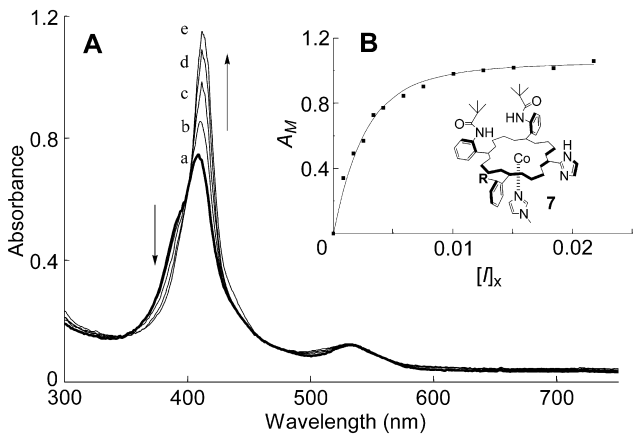

Figure 5. A: UV–vis spectral changes of dimer **5D** to monomer **7** on adding1-MeIm under N_2 in CH_2Cl_2 (**5D**: 4.0×10^{-6} M, $[1\text{-MeIm}]\times10^{-2}$: (a) 0, (b) 0.08, (c) 0.25, (d) 0.59, and (e) 2.18 M). B: Titration of absorbance of monomer **7** (A_M) at 409 nm versus $[I]_x$ (the concentration of titrated 1-MeIm). Line is a theoretical curve using K_0=2.0 for the imidazole coordination equilibrium.

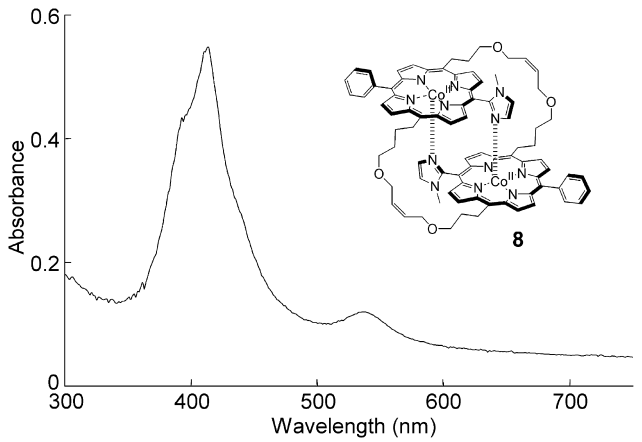

Figure 6. UV–vis spectrum of **8** in $CHCl_3$ under N_2.

$$CoPiv_3ImP + Im \overset{K_b}{\rightleftharpoons} (CoPiv_3ImP)Im \quad (2)$$

$$CoPiv_3ImP + Copiv_3ImP \overset{K_c}{\rightleftharpoons} (CoPiv_3ImP)_2 \quad (3)$$

The 1-MeIm titration curve for the peak at 409 nm was best fitted by the theoretical curve from Eq. 1 using K_a=2.0 M^{-1} (Fig. 5B).[17] Based on this value and the stability constant of K_b=1.9×10^4 M^{-1} for 1-MeIm coordination to $Co^{II}Piv_4P$,[18] the binding constant K_c (=K_b^2/K_a) for the dimer formation was evaluated as ca. 1.8×10^8 M^{-1}. This large stability constant was entirely consistent with the observation that the species exist predominantly as the dimer, 98% at 1×10^{-5} M and 95% at 1×10^{-6} M. The enhancement factor (K_c/K_b) of ca. 9.5×10^3 with the presence of porphyrin can be accounted for by the complementary nature of the coordination and the additional π stacking interaction between two porphyrins, in a similar way to the Zn complex.[1,2]

Further confirmation of the dimeric structure of ($Co^{II}Piv_3$-ImP)$_2$, **5D**, was obtained by comparing the UV–vis spectrum with that of the covalently linked imidazolyl-substituted Co(II) porphyrin dimer **8** (Fig. 6). The covalently linked imidazolyl-substituted Zn(II) porphyrin dimer, where two porphyrin components were connected by covalent bonding at the *meso* position, was previously reported.[19] Because the complementary coordination structure was frozen by covalent bonding, the structure was maintained even in the presence of a large excess of highly coordinating pyridine. Application of the same principle to Co (II) points conclusively to the dimeric structure of **8**. The UV–vis absorption spectrum of **8** in CH_2Cl_2 under N_2, presented in Figure 6, showed a broad Soret band at 414 nm (half peak width of 52 nm) with a shoulder at 395 nm and a Q band at 538 nm. The shape of this spectrum was in excellent agreement with that of $Co^{II}Piv_3ImP$. Therefore, these results suggested that $Co^{II}Piv_3ImP$, **5**, in CH_2Cl_2 formed the slipped cofacial dimeric structure ($Co^{II}Piv_3ImP)_2$, **5D**.

2.4. O_2 binding to ($Co^{II}Piv_3ImP)_2$ in UV–vis, resonance Raman, and ESR spectroscopy

The binding behavior of dioxygen was examined by introducing O_2 or N_2 gas in CH_2Cl_2 with monitoring by UV–vis spectroscopy. The spectral changes of monomer **7** generated by the addition of 1-MeIm to dimer **5D** were normal at room temperature, since the Q band at 531 nm under N_2 shifted to 542 nm under 1 atm O_2, similar to $Co^{II}Piv_4P$(1-MeIm) (530 nm under N_2, 547 nm under O_2).[6] These spectral changes were reversible. Compared to the monomer, the UV–vis spectrum of deoxy dimer **5D** did not change with introduction of O_2 at room temperature. When the temperature was lowered to 223 K under 1 atm O_2, the Soret and Q bands shifted to 412 and 547 nm, respectively. In either case, when N_2 was bubbled into the solution at 223 K or the temperature was raised up to 298 K under 1 atm O_2, the original spectrum of the deoxy state was regenerated. Therefore, the dimer showed reversible binding of dioxygen only at low temperature (223 K) (Scheme 2).

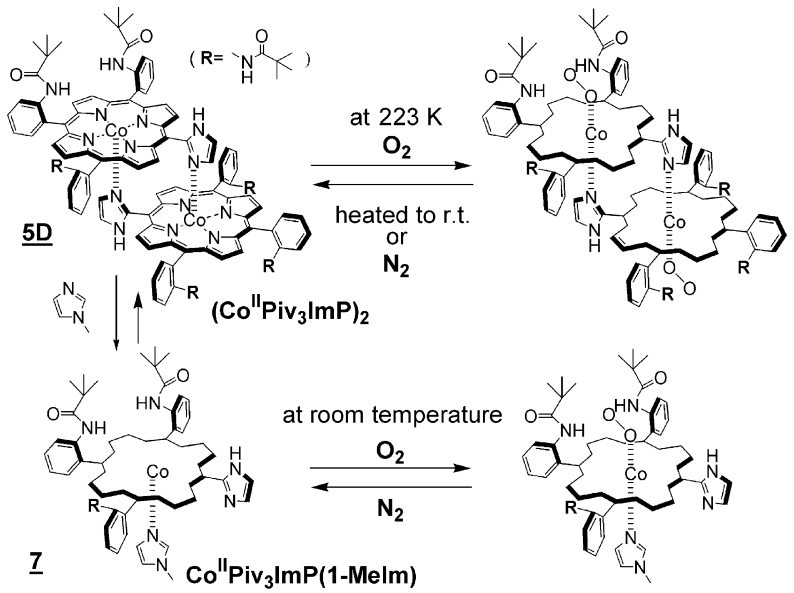

Scheme 2. Reversible dioxygen binding to dimer **5D** and monomer **7**.

In order to confirm the dioxygen binding to **5D**, resonance Raman (RR) spectroscopy was used to monitor the ν(O–O) band of the O_2 adducts.[20,21] A new band appeared at 1153 cm^{-1} under $^{16}O_2$ at 223 K, but neither at room temperature under O_2 nor at 223 K under N_2 (Fig. 7A). This band disappeared completely when the temperature was raised to 298 K, regenerating the deoxy spectrum under N_2. Under $^{18}O_2$ at 223 K, the 1153 cm^{-1} band disappeared and the intensity at 1085 cm^{-1} increased significantly (Fig. 7B). Although the 1085 cm^{-1} band was overlapped with another band, the difference in spectra under $^{16}O_2$ and under $^{18}O_2$ demonstrated clearly that the 1153 cm^{-1} band shifted to 1085 cm^{-1} (Fig. 7C), to give an isotope shift of $\Delta\nu_{obs}(^{16}O_2/^{18}O_2)$=68 cm^{-1}. This shift was nearly identical to the value calculated from the harmonic oscillator approximation for the O–O stretching vibration $\Delta\nu_{calc}(^{16}O_2/^{18}O_2)$=66 cm^{-1}, and the 1153 cm^{-1} band was assigned to $\nu(^{16}O-^{16}O)$. This value was almost the same as that observed for $\nu(^{16}O-^{16}O)$ of $Co^{II}Piv_4P$(1-MeIm), 1148 cm^{-1} in toluene at 298 K.[21]

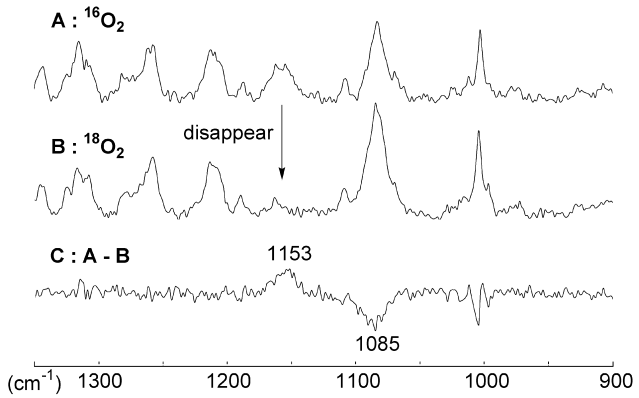

Figure 7. Resonance Raman spectra of dimer **5D** excited at 413 nm under O_2 in CH_2Cl_2 at 223 K. A: $^{16}O_2$. B: $^{18}O_2$. C: a difference spectrum of A−B.

Various dioxygen Co(II) porphyrin adducts with axial ligands have been analyzed by ESR measurements.[4,8,22] Dioxygen binding to dimer **5D** was also examined by ESR spectroscopy (Fig. 8). The ESR spectrum of dimer **5D** in toluene under N_2 at 223 K showed a single broad signal (g=2.30) analogous to that found in the spectra of Co(II) porphyrins with fifth axial ligands, for example $Co^{II}Piv_4P$(1-MeIm).[4] When dioxygen was introduced to dimer **5D** in toluene at 223 K, a new sharp peak appeared at g=2.02, which was ascribed to Co–O_2, and was accompanied by complete disappearance of the peak at g=2.30 under 1 atm O_2 (Fig. 8). The intensity changes of these two peaks at g=2.02 and 2.30 were completely correlated with each other. These results are compatible with the observations from UV–vis and RR spectra that dimer **5D** can bind dioxygen at low temperature. The complete disappearance of the peak at g=2.30 under 1 atm O_2 at 223 K indicates that the deoxy state, corresponding to a penta-coordinating Co(II) species, does not exist at all, and that the oxy state was formed 100% under these conditions. Therefore, two molecules of dioxygen can bind reversibly to the two binding sites of dimer **5D**.

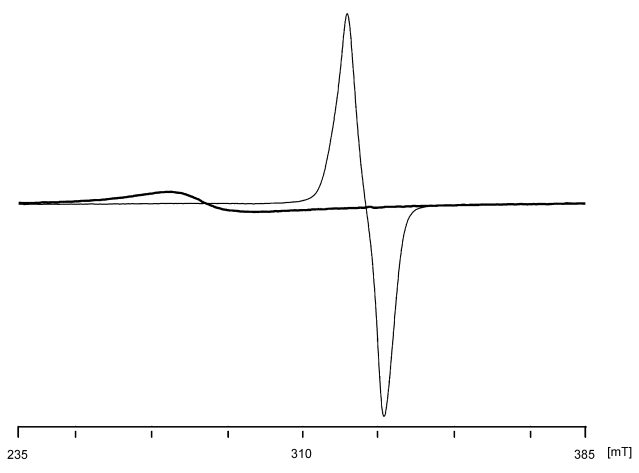

Figure 8. ESR spectral change of dimer **5D** on the addition of one atom O_2 at 223 K (narrow line) to the deoxy state (bold line) in toluene.

2.5. O_2 affinity of $(Co^{II}Piv_3ImP)_2$

The dioxygen binding equilibria of dimer **5D** are expressed as follows:

$$(CoPiv_3ImP)_2 + O_2 \overset{K_1}{\rightleftharpoons} (CoPiv_3ImP)_2O_2 \quad \text{(i)}$$

$$(CoPiv_3ImP)_2O_2 + O_2 \overset{K_2}{\rightleftharpoons} (CoPiv_3ImP)_2(O_2)_2 \quad \text{(ii)}$$

In order to determine the binding constants, K_1 and K_2, and the oxygen binding affinity $P_{1/2}$ (half-saturation oxygen pressures of O_2 binding) of dimer **5D**, UV–vis spectra were recorded at 223 K over a wide range of oxygen partial pressures using the apparatus described in Section 4. UV–vis spectra in toluene at 223 K are shown in Figure 9. From these spectra, Hill's coefficient n and $P_{1/2}$ were estimated by plotting log $Y/(1-Y)$ against log P (Y and P represent the ratio of oxy state and oxygen partial pressure, respectively). From the Hill plot, n and $P_{1/2}$ were obtained as 1.1 and 20 Torr, respectively. At first, we have expected that the dioxygen affinity of the second binding, K_2, would be different from that of the first binding, K_1. However, Hill's coefficient (n=1.1) indicates that O_2 binding to dimer **5D** is not cooperative, and K_1 is equal to K_2. From these $P_{1/2}$ values, the O_2 binding affinity of dimer **5D** is lower than those of monomeric models, for example monomer **7**, $Co^{II}Piv_4P$(1-MeIm), $Co^{II}Piv_4P$(1,2-dimethylimidazole,

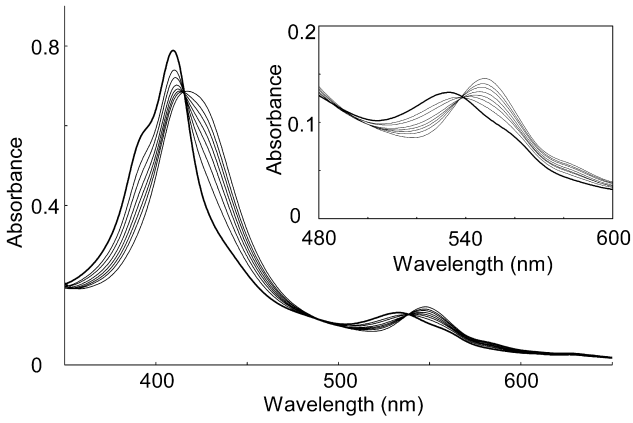

Figure 9. UV–vis spectral change of dimer **5D** on the addition of O_2 at 223 K to the deoxy state (bold line) to the oxy state (narrow line. partial pressure of O_2: 0, 7.6, 15, 23, 38, 61, 122, 760 mm Hg) in toluene. The inset is an enlarged spectral change of the Q band region.

Table 1. $P_{1/2}$ for O_2 binding to cobalt(II) porphyrins

Compound	Physical state	$P_{1/2}$ (223 K), Torr	$\Delta H°$ (kcal/mol)	$\Delta S°$ (eu)[a]	Reference
CoMb (Sperm whale)	0.1 M phosphate pH 7	0.04[b]	−13.3	−40	25
$CoPiv_4P$(1-MeIm)	Solid	0.04[b]	−13.3±0.9	−40±3	6
$CoPiv_4P$(1-MeIm)	Toluene	0.17[b]	−12.2±0.3	−38±1	6
$CoPiv_4P$(1,2-Me_2Im)	Toluene	1.1[b]	−11.8±0.4	−40±2	6
$CoPiv_3P$(1-MeIm)	Toluene	1.0[b]	−12.2	−41.6	8
($CoPiv_3$ImP)(1-MeIm) **7**	Toluene	'Very small'[c]	—	—	This work
($CoPiv_3$ImP)$_2$ **5D**	Toluene	20	—	—	This work
CoT(*p*-OCH_3)PP(1-MeIm)[d]	Toluene	106[b]	−8.9	−36	26

[a] Standard state, 1 atm O_2.
[b] Calculated from reported $\Delta H°$ and $\Delta S°$ by using equations, $\Delta H°-T\Delta S°=-RT\ln K_{eq}$, and $1/K_{eq}=P_{1/2}$.
[c] When the temperature was lowered to 223 K under N_2, a spectrum of the oxy state was obtained because a very small amount of dioxygen mingled with a cell.
[d] *meso*-Tetrakis(*p*-methoxyphenyl)porphyrinatocobalt(II)+1-MeIm.

1,2-Me_2Im), and *meso*-tetrakis(α,α,α,β-*o*-pivalamidophenyl)porphyrinatocobalt(II) with 1-MeIm, $Co^{II}Piv_3P$(1-MeIm) (see Table 1).

The decreased oxygen binding affinity of dimer **5D** compared with monomer **7** should be discussed in light of two factors. First, the axial ligand forming the complementary dimer **5D** is regarded as a 2-porphyrinyl-substituted imidazole. The steric hindrance from the 2-porphyrinyl substituent is large enough to decrease the oxygen affinity of dimer **5D**[6,7] On the other hand, the axial ligand of monomer **7** is 1-methylimidazole, which has no steric hindrance toward the porphyrin component. Hence, monomer **7** and dimer **5D** can be regarded as models for R and T forms of CoHb, respectively.This is similar to the relation between $Co^{II}Piv_4P$(1-MeIm) and $Co^{II}Piv_4P$(1,2-Me_2Im).

Secondly, the coordinating angle of the *meso*-imidazolyl groups were constrained to 45° relative to the N–Co–N axis (θ in Fig. 10) owing to the slipped cofacial complementary coordination, as shown in Figure 10A. At this orientation, the overlap between the π orbital (dπ or pπ) of Co and the pπ orbital of N on the axial base is claimed to be at a minimum,[23] and therefore the π-electron donation from the axial base to dioxygen via Co-porphyrin is reduced, decreasing the dioxygen affinity. This effect is invoked to explain the 'jellyfish' type Co(II) porphyrins.[24] On the other hand, the exogenous 1-MeIm in monomer **7** can rotate freely (Fig. 10B) and assume an angle that maximizes the π-electron donation. These two factors may explain the decreased oxygen affinity of dimer **5D** compared with monomeric models with picket fence structures, ($Co^{II}Piv_3$ImP)(1-MeIm) **7**, $Co^{II}Piv_4P$(1-MeIm), $Co^{II}Piv_4P$(1,2-Me_2Im), and $Co^{II}Piv_3P$(1-MeIm).

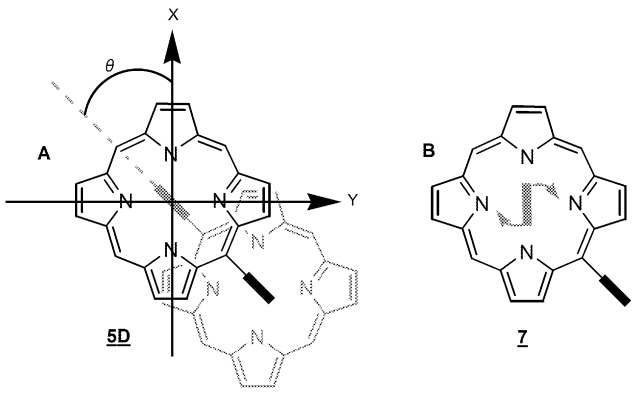

Figure 10. Schematic representation of the dihihedral angle between ligand and porphyrin axis in ($Co^{II}Piv_3ImP)_2$ **5D** and $Co^{II}Piv_3$ImP(1-MeIm) **7**. A solid bar indicates 1-MeIm.

3. Conclusion

The complementary coordination dimer of imidazolyl-substituted porphyrins was successfully and for the first time constructed into a new dioxygen carrier model, which could bind two dioxygen molecules to two binding sites of dimer **5D**. The oxygen affinity of dimer **5D** was significantly decreased compared with monomer **7**, which was obtained by adding external 1-MeIm to dimer **5D**. The relation between **5D** and **7** resembles that of hemoglobin working at lung with decreased oxygen affinity and myoglobin at terminal tissues with much higher affinity for oxygen. The significant decrease in O_2 affinity of dimer **5D** originates from the steric hindrance of the bulky 2-porphyrinyl substituent of the imidazolyl ligand and fixation at 45° of the dihedral angle between *meso*-imidazolyl ligand and the N–Co–N axis. In this way, the dioxygen affinity could readily be controlled using $Co^{II}Piv_3$ImP with the formation and dissociation of the dimeric structure.

4. Experimental

4.1. General

4.1.1. Apparatuses. ^{1}H NMR spectra were recorded on either a JEOL JNM EX 270, or a JEOL JNM-ECP 600 spectrometer. Chemical shifts are reported on a δ scale with respect to TMS as an internal standard. Coupling constants (J) are reported in Hertz (Hz). UV–vis spectra were measured by a Shimadzu UV-3100 PC spectrometer and an OXFORD OptistatDN for measurements at low temperatures with a liquid nitrogen cryostat and an OXFORD ITC502 as a temperature controller. Fluorescence spectra were recorded on a Hitachi F-4500 spectrometer. MALDI-TOF mass spectra were obtained with a PE-Biosystems Voyager-DE STR spectrometer with dithranol as a matrix. LC/HRESI(+) mass spectra were obtained with a JEOL JMS-700 (MStation) spectrometer. TLC was performed on analytical glass TLC plates coated with 60 F_{254} (E. Merck) silica gel. Column chromatography was performed using a

column packed with silica gel 60 N (Kanto Chemical, spherical, neutral, 63–210 μm). HPLC analyses of aminoporphyrins were carried out on a SHIMADZU LC-10A Series with a TOSHO TSK-gel Octadecyl-4PW column, monitored with a SHIMADZU SPD-10A UV–vis detector at 420 nm. GPC analyses were carried out on a HEWLETT–PACKARD HP 1100 Series with a JAIGEL-2.5 HA column (an exclusion limit of 2×10^4 Da), monitored by a UV–vis detector at 418 nm. Resonance Raman spectra were measured by a JASCO NRS-2100 with a COHERENT INNOVA 90C-K Kr ion laser (at 413 nm), and the temperature was controlled by a liquid nitrogen cooler system made by Daiwa Giken Co., Ltd and ourselves, and a digital thermometer (NIHON SHINTECH CT-700SD with LK-300). ESR spectra were measured on a JEOL JES-FA 100 with a temperature control unit ES-DVT4. Deoxy ($Co^{II}Piv3ImP)_2$, **5D**, and deoxy ($Co^{II}Piv3ImP$)(1-MeIm), **7**, were handled in a glove box (Miwa Seisakusho) equipped with a recycling oxygen removal system (Miwa MM3-P60S) under highly purified N_2 containing less than 0.1 ppm O_2. UV–vis titration with 1-MeIm was performed in a glove box on an Otsuka Electronics UV–vis spectrometer (MCPD-50S and MC-2530).

4.1.2. Preparation of reagents. All chemicals used in the study were of reagent grade. All dry solvents were distilled and stored under N_2. Dry THF was distilled after drying with Na metal, and CH_2Cl_2 dried with CaH_2. Dry DMF was stirred with anhydrous $CuSO_4$ for 2 days and distilled under reduced pressure from CaH_2. 1-MeIm was vacuum distilled from KOH, and 2,6-lutidine was purified by passing through an alumina column, followed by distillation from $BF_3{\cdot}Et_2O$. Anhydrous $CoCl_2$ powder was heated at 100 °C under vacuum for 30 min before use. N_2, Ar and O_2 gases were of high-quality grades (Taiyo Toyo Sanso).

4.2. Synthesis

4.2.1. 5-(2-Imidazolyl)-10,15,20-tris(*o*-nitrophenyl)-porphyrin, H_2Nitro_3ImP, (1). 2-Nitrobenzaldehyde (3.74 g, 24.8 mmol, 2 equiv.) and imidazole-2-carboxaldehyde (1.19 g, 12.4 mmol, 1 equiv.)[13] were dissolved in refluxing propionic acid (110 mL). Pyrrole (2.50 g, 37.2 mmol, 3 equiv.) was then added slowly to the boiling solution. The solution was heated under reflux for 20 min. After standing at room temperature, $CHCl_3$ (100 mL) was added to the solution, and stirred. The resulting mixture was filtered to remove *meso*-tetrakis(*o*-nitrophenyl)porphyrin and washed with $CHCl_3$. The filtrate was concentrated and purified by silica gel column chromatography, eluting with 8:1, $CHCl_3$/acetone. A purple solid of **1** was obtained, with a yield of 713 mg (0.963 mmol, 7.8%). MALDI-TOF MS *m/z* 740.4 ($M+H^+$), Calcd 740.2; UV–vis λ_{max} ($CHCl_3$) 423, 518, 555, 595, 654 nm; fluorescence λ_{Em} ($CHCl_3$) 658, 716 nm (λ_{Ex} 420 nm).

4.2.2. 5-(2-Imidazolyl)-10,15,20-tris(*o*-aminophenyl)-porphyrin, H_2Am_3ImP, (2). H_2Nitro_3ImP (**1**) (300 mg, 0.406 mmol) was dissolved in concentrated HCl (40 mL), followed by addition of excess $SnCl_2{\cdot}2H_2O$ (1.3 g). The resulting green mixture was stirred at room temperature for 30 min, and neutralized cautiously with $NaHCO_3$. Ethyl acetate was added to the suspension and the mixture was stirred. The resulting mixture was filtered under suction with addition of celite, and the residue was washed with ethyl acetate until the washings were essentially colorless. The ethyl acetate layer of the filtrate was separated, the aqueous layer extracted several times with ethyl acetate, and the extracts were combined. The ethyl acetate solution was concentrated to a smaller volume on a rotary evaporator, washed first with saturated $NaHCO_3$ solution, then twice with water and dried over anhydrous sodium sulfate. The solution was brought to dryness by a rotary evaporator and oil pump vacuum. A purple solid of the mixture of atropisomers of H_2Am_3ImP was obtained, yield 201 mg (0.309 mmol, 76%). TLC (silica gel, $CHCl_3$/MeOH, 9:1) R_f=0.55. MALDI-TOF MS *m/z* 650.4 ($M+H^+$), Calcd 650.3; UV–vis λ_{max} ($CHCl_3$) 422, 515, 556, 586, 644 nm; fluorescence λ_{Em} ($CHCl_3$) 657, 718 nm (λ_{Ex} 420 nm).

4.2.3. 5-(2-Imidazolyl)-10,15,20-tris(α,α,α-*o*-aminophenyl)porphyrin, α,α,α-H_2Am_3-ImP, (3). A mixture of atropisomers of H_2Am_3ImP (**2**) (175 mg) and 6.30 g of Kanto Chemical silica gel 60 N (63–210 μm, 600–700 m^2/g) were added to a 50 mL round-bottom flask fitted with a three-way stop-cock. The flask was evacuated with a vacuum pump for 1 h, then charged with argon gas. Toluene (15 mL) was added to the flask under a steady flow of argon gas, and argon gas was bubbled into the mixture for 10 min. The flask was attached with a reflux condenser, and immersed in an oil bath maintained at 110–120 °C, and the content was stirred under argon gas.[14] After 30 min, the slurry was cooled to room temperature and applied to the top of a silica gel chromatography column. The undesired atropisomers were eluted first with 3:1 $CHCl_3$/acetone, yield 58 mg, and then 1:1 $CHCl_3$/acetone was used to elute the α,α,α-atropisomer, yield 100 mg (57% conversion, 90% recovery). TLC (silica gel, $CHCl_3$/MeOH, 9:1) R_f=0.50. MALDI-TOF MS *m/z* 650.2 ($M+H^+$), Calcd 650.3; UV–vis λ_{max} ($CHCl_3$) 421, 517, 555, 588, 647 nm; fluorescence λ_{Em} ($CHCl_3$) 657, 716 nm (λ_{Ex} 421 nm).

4.2.4. 5-(2-Imidazolyl)-10,15,20-tris(α,α,α-*o*-pivalamidophenyl)porphyrin, H_2Piv_3ImP, (4). α,α,α-H_2Am_3-ImP (**3**) (21 mg, 0.032 mmol) was dissolved in $CHCl_3$ (2 mL), followed by addition of pyridine (10 μL) and pivaloyl chloride (10 μL, 0.112 mmol). The mixture was stirred for 1 h at room temperature, then brought to dryness on a rotary evaporator. The resulting solid was dissolved in $CHCl_3$ and the $CHCl_3$ solution was washed first with saturated $NaHCO_3$ solution, then twice with water. After drying over anhydrous sodium sulfate and reducing the volume by a rotary evaporator, the product was purified by chromatography on a silica gel column, eluting with 9:1 $CHCl_3$/acetone, yield 26 mg (0.029 mmol, 91%). MALDI-TOF MS *m/z* 902.5 ($M+H^+$), Calcd 902.4; UV–vis λ_{max} ($CHCl_3$) 421, 515, 552, 589, 649 nm; fluorescence λ_{Em} ($CHCl_3$) 655, 715 nm (λ_{Ex} 421 nm); ^1H NMR (600 MHz, $CDCl_3$) δ −2.69 (s, 2H, NH), 0.02 (s, 9H, *t*-Bu), 0.11 (s, 18H, *t*-Bu), 7.13 (s, 1H, amido), 7.25 (s, 2H, amido), 7.44 (m, 3H, benzene), 7.78 (q, 3H, benzene), 7.83 (d, *J*=6.6 Hz, 2H, benzene), 7.87 (d, *J*=6.6 Hz, 1H, benzene), 8.69 (t, 3H, benzene), 8.80 (s, 4H, pyrrole), 8.83 (d, *J*=4.4 Hz, 2H, pyrrole), 9.03 (s, 2H, pyrrole); ^{13}C NMR (600 MHz, $CDCl_3$) δ 26.44 (C43–45), 26.53 (C32–34, 54–56), 38.94 (C42), 39.05 (C31, 53), 108.47 (C5), 115.12 (C10, 20), 115.30

(C15), 120.83 (C40), 121.03 (C29, 51), 122.98 (C27, 38, 49), 130.01 (C39), 130.07 (C28, 50), 130.80 (C36), 130.92 (C25, 47), 134.23 (C37), 134.53 (C26, 48), 138.45 (C24, 46), 138.47 (C35), 146.59 (C21), 175.72 (C41), 176.11 (C30, 52).

4.2.5. 5-(2-Imidazolyl)-10,15,20-tris(α,α,α-*o*-pivalamidophenyl)porphyrinatocobalt(II) dimer, ($Co^{II}Piv_3ImP)_2$, (5D). H_2Piv_3ImP (**4**) (14 mg, 0.016 mmol) was dissolved in anhydrous THF (5 mL), followed by addition of 2,6-lutidine (30 mg, 0.310 mmol) and anhydrous $CoCl_2$ (20 mg, 0.155 mmol).[6] The mixture was stirred at 50 °C for 1 h, then brought to dryness on a rotary evaporator. The product was purified by neutral alumina (activity IV) column chromatography under N_2, eluting with 9:1 benzene/acetone, yield 11 mg (0.011 mmol, 69%). LC/HRESI(+)MS ($CHCl_3$) *m/z* 959.3692 (monomer, $M+H^+$, $C_{56}H_{54}O_3N_9Co$, Δ +1.1 ppm/+1.0 mmu), 1916.7195 (dimer, M^+, with 13% intensity relative to the monomeric peak, $C_{112}H_{106}O_6N_{18}Co_2$, Δ −0.6 ppm/+1.1 mmu); UV–vis λ_{max} (CH_2Cl_2) 389 (shoulder), 409 (ε, 1.60×10^5), 534 (1.9×10^4) nm.

4.2.6. 5-(2-Imidazolyl)-10,15,20-tris(α,α,α-*o*-pivalamidophenyl)porphyrinatocobalt(III) dimer, ($Co^{III}Piv_3ImP)_2$, (11D). ($Co^{II}Piv_3ImP)_2$ (**6D**) was dissolved in $CHCl_3$ and the solution was washed first with dilute hydrochloric acid, and then twice with water. After drying over anhydrous sodium sulfate, the solution was brought to dryness by a rotary evaporator and oil pump vacuum. The resulting solid was dissolved in a small amount of $CHCl_3$, and hexane was added dropwise to the $CHCl_3$ solution until it yielded black precipitates, and then the solution was settled over night. The resulting black precipitates were isolated by suction filtration and washed well with hexane. The product was brought to dryness on an oil pump vacuum for several hours. LC/HRESI(+)MS ($CHCl_3$) *m/z* 958.3615 (monomer, M^+, $C_{56}H_{53}O_3N_9Co$, Δ +1.2 ppm/+1.2 mmu), 1915.7109 (dimer, $M-H^+$, with intensity relative to the monomer of 16%, $C_{112}H_{105}O_6N_{18}Co_2$, Δ −1.0 ppm/−1.9 mmu); UV–vis λ_{max} (CH_2Cl_2) 328, 435, 554 nm; ^1H NMR (600 MHz, $CDCl_3$) δ −0.19 (36H, s, *t*-Bu), −0.05 (18H, s, *t*-Bu), 0.66 (2H, d, *J*=2.2 Hz, Im), 5.39 (6H, d, *J*=4.4 Hz, Im, pyrrole), 6.85 (4H, s, amido), 6.94 (2H, s, amido), 7.66 (4H, t, benzene), 7.71 (2H, t, benzene), 7.96 (6H, m, benzene), 8.29 (4H, d, *J*=7.3 Hz), 8.43 (4H, d, *J*=5.1 Hz, pyrrole), 8.49 (2H, d, *J*=7.3 Hz, benzene), 8.79 (2H, s, Im), 8.87 (4H, d, *J*=8.8 Hz, benzene), 8.97 (2H, d, *J*=8.8 Hz, benzene), 9.11 (4H, d, *J*=4.4 Hz, pyrrole), 9.22 (4H, d, *J*=4.4 Hz, pyrrole); ^{13}C NMR (600 MHz, $CDCl_3$) δ 26.59 (C32–34, 54–56, *t*-Bu), 26.72 (C43–45, *t*-Bu), 38.83 (C31, 53, *t*-Bu), 38.96 (C42, *t*-Bu), 98.79 (C5, *meso*), 113.28 (C22, Im), 115.44 (C10, 20, *meso*), 115.81 (C15, *meso*), 120.49 (C29, 40, 51, benzene), 122.50 (C38, benzene), 122.80 (C27, 49, benzene), 124.52 (C23, Im), 129.73 (C3, 7, pyrrole-β), 129.96 (C36, benzene), 130.21 (C39, benzene), 130.28 (C25, 47, benzene), 130.31 (C28, 50, benzene), 133.76 and 133.82 (C26, 48, benzene, or H12, 18, pyrrole-β), 134.71 (C37, benzene), 134.80 (C13, 17, pyrrole-β), 134.99 (C2, 8, pyrrole-β), 138.62 (C24, 46, benzene), 138.94 (C35, benzene), 143.94, 144.18, 144.96 (pyrrole-α), 145.25 (C21, Im), 145.52 (pyrrole-α), 176.59 (C30, 53, C═O), 176.64 (C41, C═O).

4.2.7. Covalently linked imidazolyl-substituted Co(II) porphyrin dimer, (8). Covalently linked imidazolyl-substituted Zn(II) porphyrin dimer[19] (9 mg, 6.45 μmol) was dissolved in $CHCl_3$ (3 mL). The solution was added to a MeOH/HCl (1:1) mixture (0.5 mL), stirred for 30 min and washed, first with saturated $NaHCO_3$ solution and then twice with water and subsequently dried over anhydrous sodium sulfate. The solution was dried completely on a rotary evaporator and then oil pump vacuum. A purple solid of covalently linked freebase porphyrin dimer was obtained, with a yield of 11 mg. The product (11 mg) was dissolved in anhydrous THF (3 mL), followed by addition of 2,6-lutidine (30 mg) and anhydrous $CoCl_2$ (20 mg). The mixture was stirred at 70 °C for 1 h under N_2, then dried on a rotary evaporator. The product was purified by neutral alumina (activity IV) column chromatography under N_2, eluted with 3:1 benzene/MeOH, yield 7 mg (5.06 μmol, 78%). MALDI-TOF MS *m/z* 1383.5 ($M+H^+$), Calcd 1382.5; UV–vis λ_{max} (CH_2Cl_2) 395, 414, 538 nm.

4.3. Measurement techniques

4.3.1. UV–vis titration of ($Co^{II}Piv_3ImP)_2$ with 1-MeIm. All operations were conducted in a glove box. A solution of ($Co^{II}Piv_3ImP)_2$ **5D** in CH_2Cl_2 (4.2×10^{-6} M, 3 mL) was injected into a cell having a plug (cell path length was 10 mm). The solution of 1-MeIm in CH_2Cl_2 (2.5 M) was titrated into the cell by micro syringe, and the resulting solution was stirred for 3 min and its UV–vis absorbance was measured. When, A, ε, M, and D represent absorbance, molar absorption coefficient, monomer **7**, and dimer **5D**, respectively, the following equations hold.

$$A = A_M + A_D = \varepsilon_M[M] + \varepsilon_D[D] \tag{4}$$

$$[D] = [D]_0 - \frac{[M]}{2} = [D]_0 - \frac{A_M}{2\varepsilon_M} \tag{5}$$

Since the initial solution is considered to contain dimer only, we assume Eq. 6.

$$A_0 = \varepsilon_D[D]_0 \tag{6}$$

These relations lead to Eq. 7:

$$A_M = \frac{2\varepsilon_M(A - A_0)}{2\varepsilon_M - \varepsilon_D} \tag{7}$$

The value of ε_M was evaluated from the absorption at the final titration point.

Eq. 8 is obtained by the definition of Eq. 1, where [I] is the concentration of 1-MeIm and rewritten in the form of Eq. 9.

$$K_a = \frac{[M]^2}{[D]\times[I]^2} = \frac{[M]^2}{([D]_0 - [M]/2)([I]_x - [M])^2} \tag{8}$$

$$K_a = \frac{(A_M/\varepsilon_M)^2}{(A_0/\varepsilon_D - A_M/2\varepsilon_M)([I]_x - A_M/\varepsilon_M)^2} \tag{9}$$

In Figure 6B, A_M at 409 nm was plotted as a function of $[I]_x$, the concentration of titrated 1-MeIm. The best fit K_0 value was evaluated as 2.0 M^{-1}.

4.3.2. Oxygen equilibria. A solution of ($Co^{II}Piv_3ImP)_2$, **5D**, in toluene (4.9×10^{-6} M) was injected into a cell (cell path

length 10 mm) and sealed by a rubber septum in a glove box. The cell was inserted into a liquid nitrogen cryostat, and the UV–vis absorption spectrum was measured at 223 K. Gas mixtures of N_2 and O_2 of various compositions were prepared by a KOFLOC GASCON GM-3B, and their oxygen partial pressures were monitored by a TORAY OXYGEN ANALYZER LC-850 KS. The gas mixture was bubbled into the sample solution through a needle for 5 min before measurements. From the spectra (Fig. 9), Hill's coefficient n and $P_{1/2}$ were estimated by plotting $\log Y/(1-Y)$ versus $\log P$.

$$\log\frac{Y}{1-Y} = \log\frac{A_{oxy}/A_{100\%}}{1-(A_{oxy}/A_{100\%})} = \log\frac{A_{oxy}}{A_{100\%}-A_{oxy}} \quad (10)$$

Y is the oxy state composition calculated by $A_{oxy}/A_{100\%}$, where A_{oxy} and $A_{100\%}$ represent the absorbance of the oxy state at 537 nm and that under 760 Torr O_2, respectively. A_{oxy} was calculated by using the equations shown below.

$$A = A_{oxy} + A_{deoxy} = \varepsilon_{oxy}[oxy] + \varepsilon_{deoxy}[deoxy] \quad (11)$$

$$[deoxy] = [deoxy]_0 - [oxy] = [deoxy]_0 - \frac{A_{oxy}}{\varepsilon_{oxy}} \quad (12)$$

where oxy and deoxy represent oxy and deoxy states, respectively. Since the initial solution is considered to contain only the deoxy state, Eq. 13 holds.

$$A_0 = \varepsilon_{deoxy}[deoxy]_0 \quad (13)$$

These relations (11)–(13) lead Eq. 14:

$$A_{oxy} = \frac{\varepsilon_{oxy}(A-A_0)}{\Delta\varepsilon} \quad (14)$$

where $\Delta\varepsilon$ is the difference between molar absorption coefficients of the oxy and the deoxy states. Finally, Eq. 15 is obtained by substitution of Eq. 14 into Eq. 10.

$$\log\frac{Y}{1-Y} = \log\frac{\varepsilon_{oxy}(A-A_0)}{\Delta\varepsilon A_{100\%} - \varepsilon_{oxy}(A-A_0)} \quad (15)$$

Hill's coefficient n was estimated by a slope of the straight line, which was obtained by using a linear least-squares program of the Hill's plot. $P_{1/2}$ was determined from the intercept at the x-axis.

Acknowledgements

We thank Ms. Yoshiko Nishikawa, a technical official of Nara Institute of Science and Technology, for the measurements of LC/HRESI(+) mass spectra. We gratefully acknowledge Japan Science and Technology Agency (JST) for support of this work.

References and notes

1. (a) Kobuke, Y.; Miyaji, H. *J. Am. Chem. Soc.* **1994**, *116*, 4111–4112. (b) Ozeki, H.; Kobuke, Y. *Tetrahedron Lett.* **2003**, *44*, 2287–2291.
2. Kobuke, Y.; Ogawa, K. *Bull. Chem. Soc. Jpn.* **2003**, *76*, 689–708.
3. (a) Collman, J. P.; Fu, L. *Acc. Chem. Res.* **1999**, *32*, 455–463. (b) Suzuki, Y.; Nishide, H.; Tsuchida, E. *Macromolecules* **2000**, *33*, 2530–2534.
4. Collman, J. P.; Gagne, R. R.; Kouba, J.; Ljusberg-Wahren, H. *J. Am. Chem. Soc.* **1974**, *96*, 6800–6802.
5. Collman, J. P.; Gagne, R. R.; Reed, C. A.; Halbert, T. R.; Lang, G.; Robinson, W. T. *J. Am. Chem. Soc.* **1975**, *97*, 1427–1439.
6. Collman, J. P.; Brauman, J. I.; Doxsee, K. M.; Halbert, T. R.; Hayes, S. E.; Suslick, K. S. *J. Am. Chem. Soc.* **1978**, *100*, 2761–2766.
7. Collman, J. P.; Brauman, J. I.; Doxsee, K. M.; Halbert, T. R.; Suslick, K. S. *Proc. Natl Acad. Sci. U.S.A.* **1978**, *75*, 564–568.
8. Imai, H.; Nakata, K.; Nakatsubo, A.; Nakagawa, S.; Uemori, Y.; Kyuno, E. *Synth. React. Inorg. Met.-Org. Chem.* **1983**, *13*, 761–780.
9. (a) Tabushi, I.; Sasaki, T. *J. Am. Chem. Soc.* **1983**, *105*, 2901–2902. (b) Tabushi, I.; Kugimiya, S.; Kinnaird, M. G.; Sasaki, T. *J. Am. Chem. Soc.* **1985**, *107*, 4192–4199.
10. (a) Uemori, Y.; Nakatsubo, A.; Imai, H.; Nakagawa, S.; Kyuno, E. *Inorg. Chim. Acta* **1986**, *124*, 153–160. (b) Uemori, Y.; Munakata, H.; Shimizu, K.; Nakatsumo, A.; Imai, H.; Nakagawa, S.; Kyuno, E. *Inorg. Chim. Acta* **1986**, *113*, 31–36.
11. (a) Traylor, T. G.; Tatsuno, Y.; Powell, D. W.; Cannon, J. B. *J. C. S. Chem. Commun.* **1977**, 732–734. (b) Traylor, T. G.; Mitchell, M. J.; Ciccone, J. P.; Nelson, S. *J. Am. Chem. Soc.* **1982**, *104*, 4986–4989.
12. Salmon, L.; Bied-Charreton, C.; Gaudemer, A.; Moisy, P.; Bedioui, F.; Devynck, J. *Inorg. Chem.* **1990**, *29*, 2734–2740.
13. (a) Iverson, P. E.; Lund, H. *Acta Chem. Scand.* **1966**, 2649. (b) Curtis, N. J.; Brown, R. S. *J. Org. Chem.* **1980**, *45*, 4038–4040.
14. Lindsey, J. *J. Org. Chem.* **1980**, *45*, 5215.
15. (a) Smith, K. M.; Bobe, F. W.; Goff, D. A.; Abraham, R. J. *J. Am. Chem. Soc.* **1986**, *108*, 1111–1120. (b) Stibrany, R. T.; Vasudevan, J.; Knapp, S.; Poterza, J. A.; Emge, T.; Schugar, H. J. *J. Am. Chem. Soc.* **1996**, *118*, 3980–3981.
16. Shirazi, A.; Goff, H. M. *Inorg. Chem.* **1982**, *21*, 3420–3425.
17. If the initial species before 1-MeIm titration exists as monomer **10** in CH_2Cl_2, the coordination equilibria are expressed as Eq. (2). The theoretical curve using various K cannot fit the experimental values at all. Therefore, the initial species must correspond to dimer **10D**.
18. Imai, H.; Kyuno, E. *Inorg. Chem. Acta* **1988**, *153*, 175–182.
19. Ohashi, A.; Satake, A.; Kobuke, Y. *Bull. Chem. Soc. Jpn.* **2004**, *77*, 365–374.
20. (a) Mackin, H. C.; Tsubaki, M.; Yu, N. T. *Biophys. J.* **1983**, *41*, 349–357. (b) Nakayama, S.; Tani, F.; Matsu-ura, M.; Naruta, Y. *Chem. Lett.* **2002**, *31*, 496.
21. Odo, J.; Imai, H.; Kyuno, E.; Nakamoto, K. *J. Am. Chem. Soc.* **1988**, *110*, 742–748.
22. (a) Walker, F. A. *J. Am. Chem. Soc.* **1970**, *92*, 4235–4244. (b) Däges, G. P.; Hüttermann, J. *J. Phys. Chem.* **1992**, *96*, 4787–4794. (c) Bowen, J. H.; Shokhirev, N. V.; Raitsimring, A. M.; Buttlaire, D. H.; Walker, F. A. *J. Phys. Chem. B* **1997**, *101*, 8683–8691.
23. Scheidt, W. R.; Chipman, D. M. *J. Am. Chem. Soc.* **1986**, *108*, 1163–1167.
24. Uemori, Y.; Miyakawa, H.; Kyuno, E. *Inorg. Chem.* **1988**, *27*, 377–382.
25. (a) Hoffman, B. M.; Petering, D. H. *Proc. Natl Acad. Sci. U.S.A.* **1970**, *67*, 637–643. (b) Spilburg, C. A.; Hoffman, B. M.; Petering, D. H. *J. Biol. Chem.* **1972**, *247*, 4219–4223.
26. (a) Walker, F. A. *J. Am. Chem. Soc.* **1973**, *95*, 1150–1153. (b) Walker, F. A. *J. Am. Chem. Soc.* **1973**, *95*, 1154–1159.